Modeling and Simulation of High Blocking Voltage in 4H Silicon Carbide Bipolar Junction Transistors

.

ABSTRACT

For a given breakdown voltage, the drift region thickness and doping concentration of punch-through structure can be optimized to give the lowest specific on-resistance. An optimization scheme performed for a breakdown voltage of 14 kV in 4H-SiC bipolar junction transistor (BJT) at 300 °K. The optimum drift region thickness and doping concentration for a 4H-SiC punch-through structure at different breakdown voltages are presented. The optimum drift region thickness and doping concentration are 114 *μm* and $6.6\times10^{14}cm^{-3}$, respectively, which results in the lowest specific on-resistance of 117 mΩcm^2. The specific on-resistance is compared with the theoretical specific on-resistance of non punch-through structure. It is shown that the optimized punch-through structure not only has a thinner drift region, but also has a slightly lower specific on-resistance than non punch-through structure. The model is applied and compared to a measured 4H-SiC bipolar transistors with high blocking voltage and results are discussed. The experimental 4H-SiC BJT is able to block 1631 V and 2033 V at 300 °K and 523 °K when the base is open, respectively. The simulated blocking voltage when base is open is slightly lower, 1600 V at 300 °K, than the experimental value due to the current-amplifying properties of the common-emitter BJT.

Keywords: Device Modeling, Silicon Carbide, Bipolar Junction Transistors

1. Introduction

Although many improvements have been made in silicon material technology and in the design of new device structures, the silicon-based power devices are rapidly approaching their theoretical limits of performance [1,2].

As shown in Table 1, when compared to silicon, 4H-SiC offers a lower intrinsic carrier concentration (9 to 37 orders of magnitude), a higher electric breakdown field (4 to 18 times), a higher thermal conductivity, and a larger saturation electron drift velocity 2 to 2.7 times higher [3-6]. Because of high electric breakdown field, the drift region can be much thinner than that of their Si counterparts for the same voltage rating, thus a much lower specific on-resistance could be obtained. With lower specific on-resistance, wide-bandgap-based power devices have lower conduction losses and higher overall efficiency. Because of high-saturation drift velocity power devices based on wide-bandgap materials could be switched at higher frequencies than their Si counterparts. Moreover, the charge in the depletion region of a PN junction can be removed faster if the drift velocity is higher, and therefore, the reverse recovery time is shorter.

Table 1. Physical parameters and bias variables

Physical Parameters and Variables	Unit	Value
Electron mobility, μ_n	cm^2/V-s	347
Hole mobility, μ_p	cm^2/V-s	34.5
Electron lifetime, τ_n	ns	22
Hole lifetime, τ_p	ns	5.7
Collector series resistance, R_C	Ω	1.24
Collector-Emitter Bias, V_{CE}	V	-
Collector Current, I_C	A	-
Base Current, I_B	A	-

Breakdown electric field in 4H-SiC is almost one order of magnitude higher than silicon, which makes 4H-SiC superior in high voltage applications. This high breakdown electric field allows 4H-SiC power devices use a much thinner and higher-doped drift layer, hence significantly reduces the device specific on-state resistance which reduces the conduction loss significantly [7, 8].

Because of high saturation drift velocity, 4H-SiC power devices have higher current density and switch faster than silicon. Together with its superior thermal conductivity, wide band-gap, and low on-state resistance, 4H-SiC power devices could be much smaller in size while providing comparable amount of power output.

The fabrication and characterization of a 4H SiC bipolar junction transistor with double base epilyer is reported in [9,10]. The control of the etch depth and the formation of a low-resistive p-type ohmic contact to the epitaxial base is shown to be the key in their fabrication and design technique that can be used to improve specific on-resistance and the breakdown voltage. The ATLAS device simulation tool was used to investigate the electrical characteristics of a 4H-SiC bipolar junction transistor [11]. The lateral BJT structure with surface electric field optimization technique is shown to achieve a high breakdown voltage and lower specific on resistance [12]. It is shown that the base electric field plate can restrict collector-base depletion extension in the base region. They were able to show that high avalanche breakdown can be obtained at high current gain in device structures with lateral thin base and low base doping. A SiC thyristor is reported where a high voltage breakdown voltage of 8.7 kV is obtained using a much thicker drift layer [13]. The multiple-floating-zone junction termination and improved diffusion techniques are new fabrication techniques used by several investigators to achieve high blocking voltage that approach near the ideal breakdown values in SiC bipolar transistors[14]. A breakdown voltage of 21.7 kV is achieved in 4H-SiC PiN diodes with improved junction termination extension structures and by using a space-modulated structure where a wide termination window tailoring the doping dose to compensate the impact of interface charge [15]. This planar termination window is produced by implantation of fine-scale areas of dopant, followed by diffusion to smooth out the dopant profile where the surface field remains below breakdown voltage [16]. Numerical device simulations have been performed for over 15-kV-class 4H-SiC p-i-n diodes with an edge termination method. The structure exhibited a high breakdown capability with an improved tolerance for the deviation of impurity dose in the junction termination region which made it feasible for of various high-voltage devices in 4H-SiC [17]. Due to the advantages of 4H-SiC devices such as low specific on-resistance, high thermal stability, and high blocking voltage, SiC MOSFET and BJTs are expected to replace Si IGBT [18, 19, 20]. Similarly, the use field-plate structure is also used in other material system such as Gallium Nitride for power device applications to achieve high blocking voltage and low specific on-resistance [21-24].

We report that the breakdown characteristics of 4H-SiC junction transistors can be severely affected by both the drift region thickness and the doping density. In this study, the two-dimensional numerical analysis tool ATLAS [11] is used to investigate the electrical characteristics in 4H-SiC bipolar transistors. The simulation and theoretical model are compared to the measured 4H-SiC bipolar junction transistors. An optimization model is presented to obtain the lowest specific on-resistance. It can be shown that the punch-through structure not only has a thinner drift region, but also can have a slightly lower specific on-resistance than non punch-through structure. It is shown that the simulated blocking voltage is slightly lower when base is open due to the current-amplifying properties of the common-emitter bipolar junction transistors.

2. Modeling Ionization Coefficients

Recently 4H-SiC bipolar junction transistors with a blocking voltage in the range of 0.75 kV to 9.2 kV and with an on-state resistance of 2.9 mΩcm^2 to 49 mΩcm^2 are reported [25, 26, 27]. In high electric field, free carriers can obtain enough energy to cause impact ionization. This process can be understood as the inverse process to the Auger recombination. The reciprocal of the carrier mean free path is called the impact ionization coefficient. With these coefficients of electrons and holes, the generation rate G due to impact ionization can be expressed as

$$G = \alpha_n n v_n + \alpha_p n v_p \qquad (1)$$

where α_n and α_p denote the impact ionization coefficients of electrons and holes, v_n and v_p are the electron and hole drift velocities, receptively. α_n and α_p are modeled with Chynoweth equation [28]:

$$\alpha(E) = \gamma\alpha_0 \exp\left(-\frac{\gamma b}{E}\right) \quad (2)$$

where *E* is the electric field and α_0 and *b* are fitting parameters:

$$\gamma(T) = \frac{\tanh\left(\frac{h\omega_{op}}{2kT_0}\right)}{\tanh\left(\frac{h\omega_{op}}{2kT}\right)} \quad (3)$$

The parameter γ and the optical phonon energy $h\omega_{op}$ relate the temperature dependence of phonon gas against the accelerated carriers. Both $\gamma\alpha_0$ and γb should depend on lattice temperature (T). However, the term γb is shown experimentally to be independent of the temperature in SiC [29]. Therefore, the empirical model suggested by Okuto and Crowell is used [30]:

$$\alpha(E) = a \cdot \left[1 + c \cdot (T - 300K)\right] \cdot E^{\gamma_1} \cdot \exp - \left[\frac{b \cdot (1 + d \cdot (T - 300K))}{E}\right]^{\gamma_2} \quad (4)$$

where *a*, *b*, *c*, *d*, γ_1 and γ_2 are fitting parameters.

Two sets of the experimental measurements on 4H-SiC impact ionization coefficients were reported. The hole impact ionization coefficient α_p reported in [31] which was measured by using e-beam induced current, is much smaller than that reported in [29] which was measured by direct measurements of avalanche photodiodes. Monte Carlo simulation [14] [shows that there is a significant anisotropy in the impact ionization coefficients in 4H-SiC. The impact ionization coefficients for transport perpendicular to c-axis are from 5 to 10 times greater than the values for transport parallel to c-axis. This implies that the breakdown voltage is mainly determined by the breakdown perpendicular to c-axis if the electric field strengths in the direction parallel and perpendicular to c-axis are approximately equal, as is the case for most practical SiC devices. The anisotropy in the impact ionization coefficients, however, has not been implemented in the Atlas simulator [11] so it is customary in the simulations to select a set of impact ionization coefficients between the impact ionization coefficients in c-axis and perpendicular to c-axis. The measured hole impact ionization coefficients in [29] are in good agreement with Monte Carlo simulation results in the direction of c-axis. The measured impact ionization coefficients in [31] lie between the Monte Carlo results parallel to c-axis and perpendicular to c-axis. As a result the measured impact ionization coefficients in [31] are used to predict the blocking voltage in this paper, where the measured temperature dependence reported in [29] is applied. In this way, it is assumed that the temperature coefficients of the impact ionization coefficients are the same in the direction parallel to c-axis and perpendicular to c-axis. By fitting the experimental results in with Eq. (4), the impact ionization coefficients α_n and α_p are expressed as below:

$$\alpha_n\left(E,T\right)=7.26\times10^{6}\left(1-1.47\times10^{-3}\left(T-300K\right)\right)\exp\left(-\frac{2.34\times10^{7}}{E}\right)cm^{-1} \tag{5}$$

$$\alpha_p\left(E,T\right)=6.85\times10^{6}\left(1-1.56\times10^{-3}\left(T-300K\right)\right)\exp\left(-\frac{1.41\times10^{7}}{E}\right)cm^{-1} \tag{6}$$

2.1 Critical Field of 4H-SiC Power Transistors

For power devices, the high blocking voltage is usually supported by a thick lightly doped drift layer. Since the drift layer is thick and low-doped, its resistance may dominate the on-resistance of the power device.

The avalanche breakdown due to impact ionization will occur when the electric field exceeds the critical field (E_{cr}):

$$E_{cr}=\frac{2.49\times10^{6}}{1-\frac{1}{4}\log_{10}\left(\frac{N}{10^{16}cm^{-3}}\right)}V/cm \tag{7}$$

where N is the doping concentration. The critical field in 4H-SiC is dependent on the doping concentration, as shown in Figure 1. The critical field in 4H-SiC is 3 MV/cm at a doping concentration $5\times10^{16}cm^{-3}$, which is 10 times higher than in silicon.

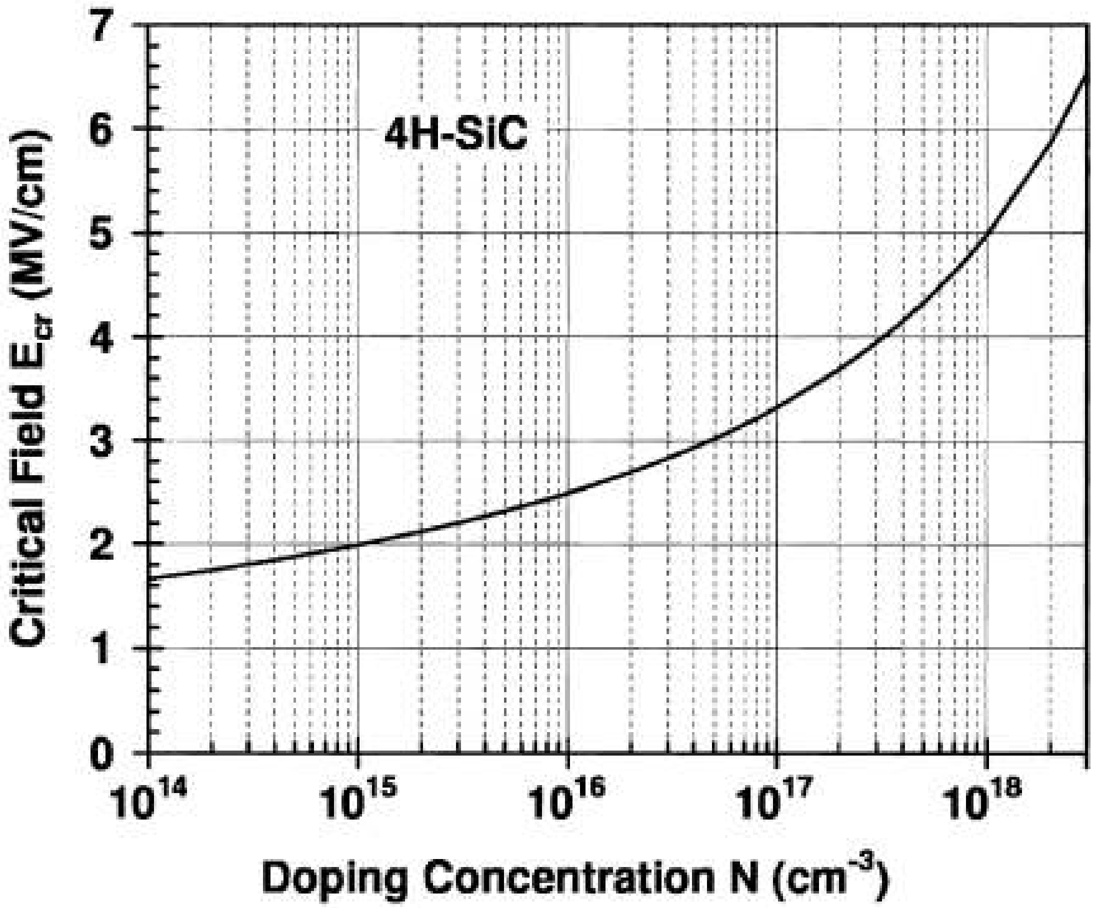

Figure 1. Dependence of the critical field in 4H-SiC on the doping concentration.

2.2 Drift Layer Design for Non-Punch-Through Structure

For a power device with an n-type lightly doped drift layer, the blocking junction can be approximated with a one-side abrupt P^+N junction. In the blocking state the depletion region mainly extends into the lightly doped drift region. The maximum electric field in the depletion region is given by:

$$E_{\max} = \sqrt{\frac{2qN_D V_a}{\varepsilon_s}} \tag{8}$$

where V_a is the applied voltage, N_D is the drift layer doping concentration and ε_s is the dielectric constant of the semiconductor. From this equation, it can be seen that the maximum electric field in the depletion region increases with increasing applied bias. The breakdown voltage V_{BR} can be derived from Eq. (8):

$$V_{BR} = \frac{\varepsilon_s E_{cr}^2}{2qN_D} \tag{9}$$

Therefore, for the non-punch-through structure, the doping level N_D required to support a given breakdown voltage V_{BR} can be determined from Eq. (9):

$$N_D = \frac{\varepsilon_s E_{cr}^2}{2qV_{BR}} \tag{10}$$

The drift layer thickness should be larger than the maximum width of the depletion region at breakdown:

$$W = \sqrt{\frac{2\varepsilon_s V_{BR}}{qN_D}} = \frac{2V_{BR}}{E_{cr}} \tag{11}$$

Thus, the theoretical specific on-resistance R_{SP_ON} associated with the drift layer is

$$R_{SP\_ON} = resistance \cdot area = \frac{W}{q\mu_n N_D} = \frac{4V_{BR}^2}{\varepsilon_s \mu_n E_{cr}^3} \tag{12}$$

where μ_n is the drift layer electron mobility. It is seen from the above equation that the value of V_{BR}^2 / R_{SP_ON} is only dependent on the material properties:

$$V_{BR}^2 / R_{SP\_ON} = \frac{1}{4}\varepsilon_s \mu_n E_{cr}^3 \tag{13}$$

Thus, the value of V_{BR}^2 / R_{SP_ON} is often used to evaluate how close the performance of a fabricated power device approaches the material limit.

For silicon, the drift layer doping concentration and thickness required to support a given breakdown voltage are given by [32, 33]:

$$N_D = 2.01 \times 10^{18} V_{BR}^{-4/3} \tag{14}$$

and

$$W = 2.58 \times 10^{-6} V_{BR}^{7/6}, \tag{15}$$

Where, the theoretical specific on-resistance of silicon drift layer in Ωcm^2 is

$$R_{SP\_ON} = 5.98 \times 10^{-9} V_{BR}^{2.5} \tag{16}$$

The theoretical specific on-resistance for 4H-SiC drift layer is presented in Figure 2. For comparison the theoretical specific on-resistance of silicon drift-layer is also shown.

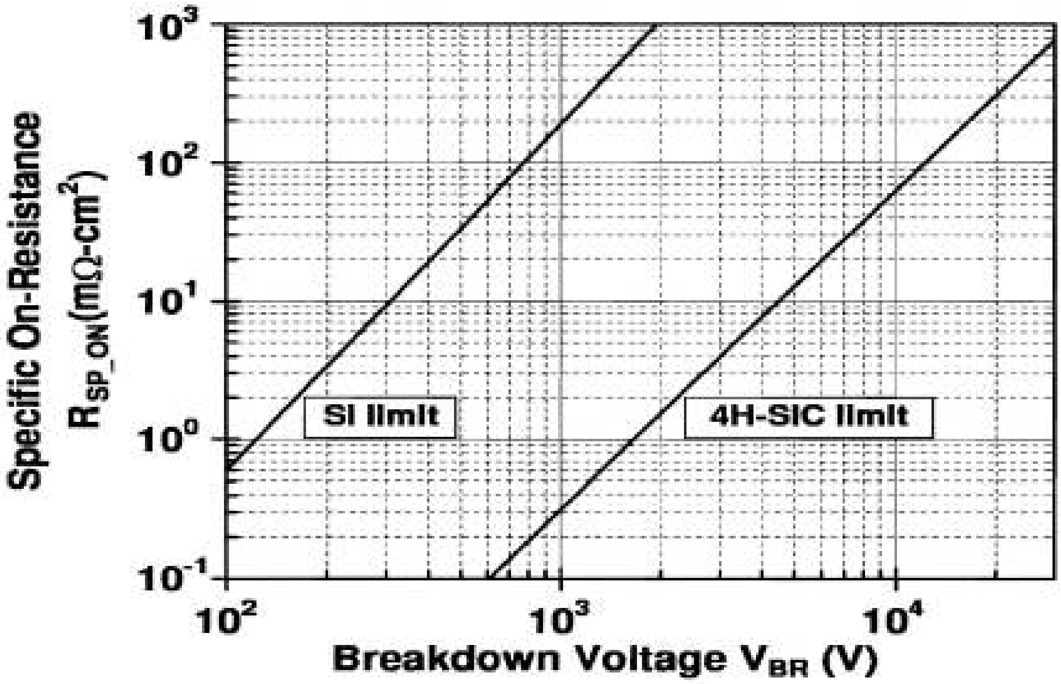

Figure 2. Theoretical specific on-resistance of silicon and 4H-SiC drift layers at different voltage ratings.

It can be seen that the specific on-resistance of SiC drift layer can be about 550 times lower than that of silicon drift layer for the same voltage rating due to the higher critical field in SiC. Figure 3a presents the breakdown voltage and the depletion region width at breakdown as a function of the doping concentration N_D for 4H-SiC. For a given breakdown voltage, the required drift layer doping concentration and thickness can be determined from Figure 3b.

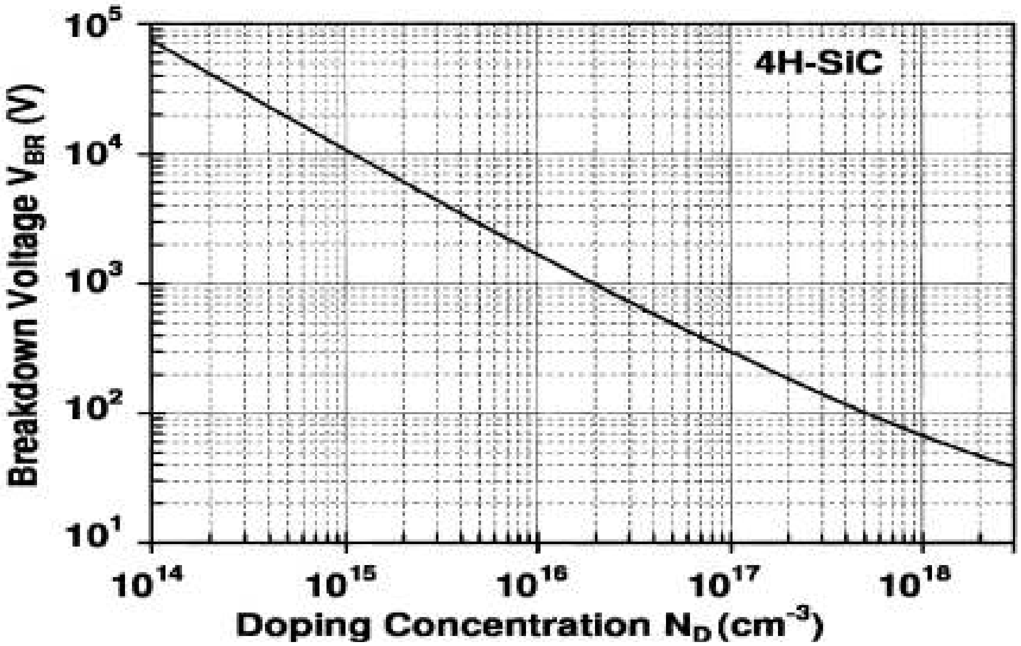

(a)

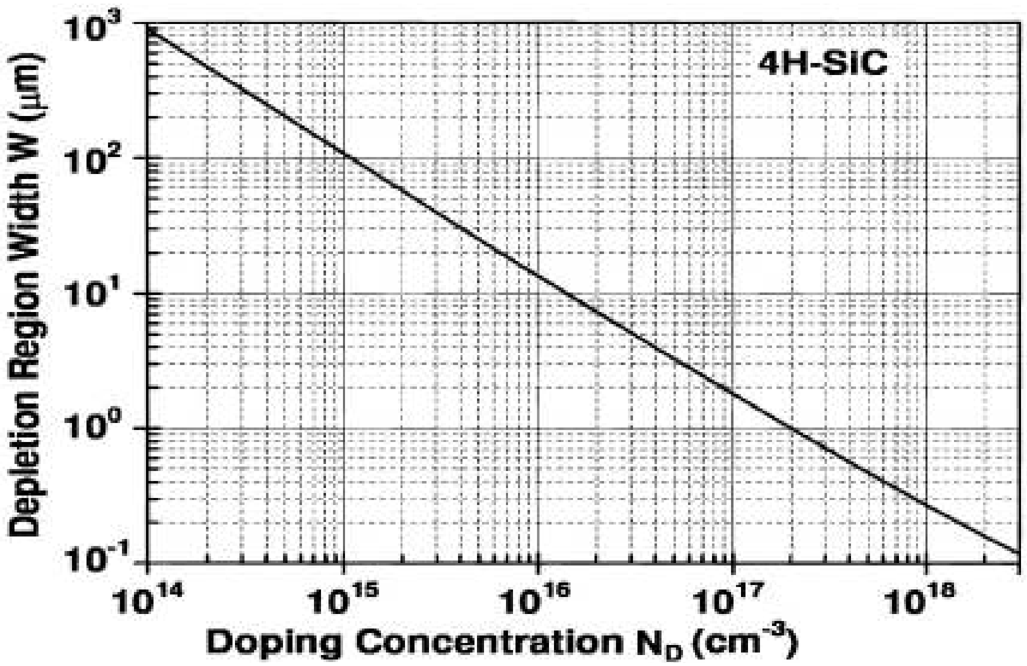

(b)

Figure 3. Dependence of the breakdown voltage (a) and the depletion region width at breakdown (b) on the drift layer doping concentration of one-sided abrupt P^+N junction.

2.3 Drift Layer Design for Punch-Through Structure

For most power devices, it is preferable to use a punch-through structure to support the voltage, as shown in Figure 4. In general, the punch-through structure has a lower doping concentration on the lightly doped side with a high concentration contact region, and the thickness of the lightly doped side is smaller than that for non punch-through structure for equal breakdown voltages. In punch-through structure, the electric field varies less gradually with distance within the lightly doped region, resulting in a rectangular electric field profile as compared to a triangular electric field profile for the non punch-through structure, as illustrated in Figure 4. The breakdown voltage for punch-through structure is given by [32]:

$$V_{BR} = E_{cr}W_P - \frac{qN^{-}W_p^2}{2\varepsilon_s} \qquad (17)$$

where W_p and N^{-} are the thickness and doping concentration of the drift region (lightly doped region), respectively. Figure 5 shows the breakdown voltage calculated for the punch-through structure in 4H-SiC as a function of the drift region doping concentration. When the doping concentration and the thickness of the drift region become large, the breakdown voltage approaches that for the non punch-through structure. In addition, the breakdown voltage of the punch-through structure is a weak function of the drift region doping concentration if its thickness is small.

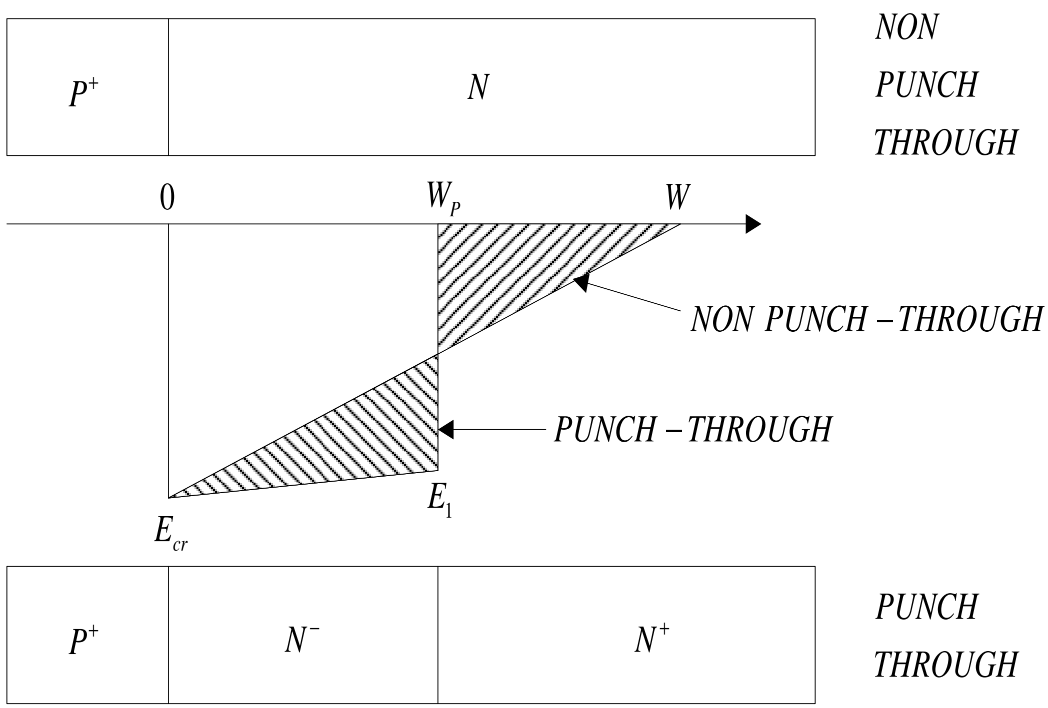

Figure 4. Comparison of punch-through structure with non punch-through structure.

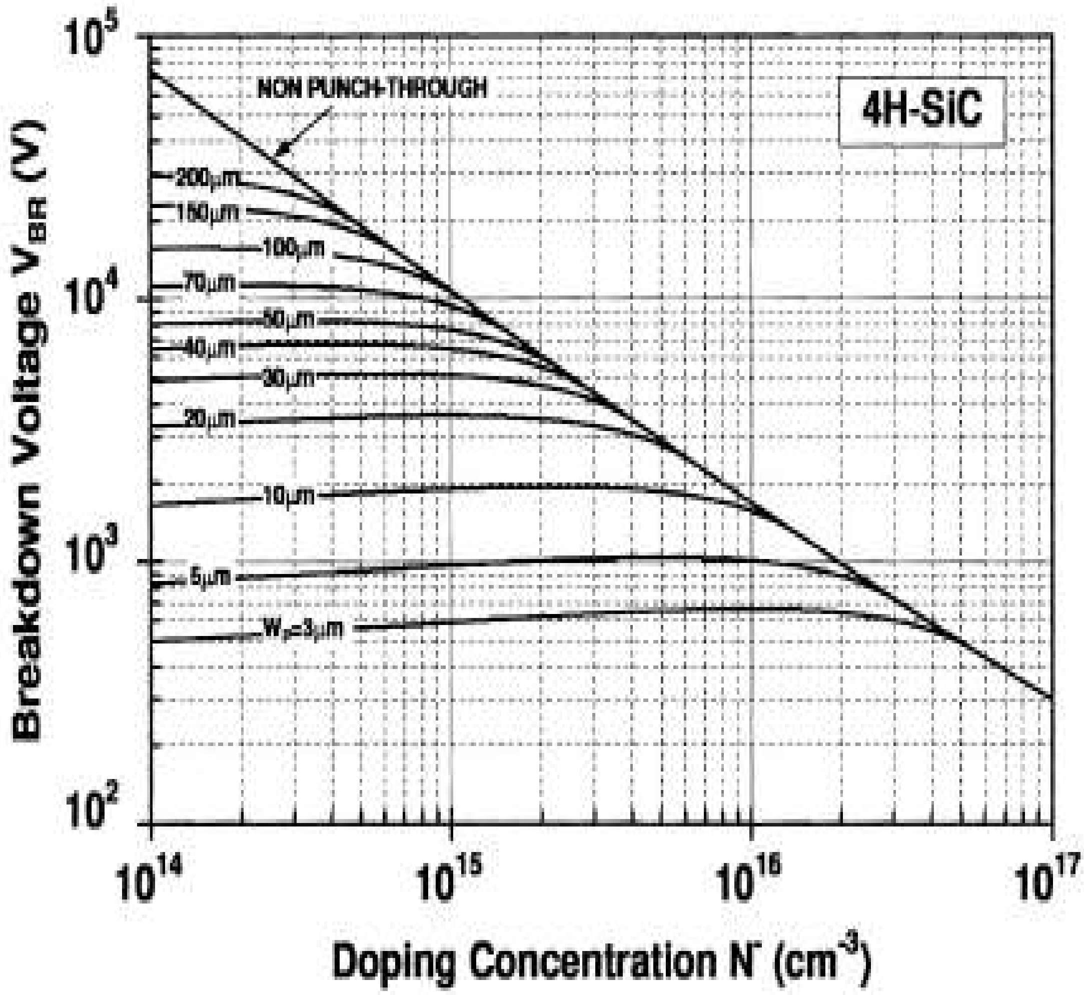

Figure 5. Dependence of the breakdown voltages in 4H-SiC punch-through structures on the drift region doping concentration.

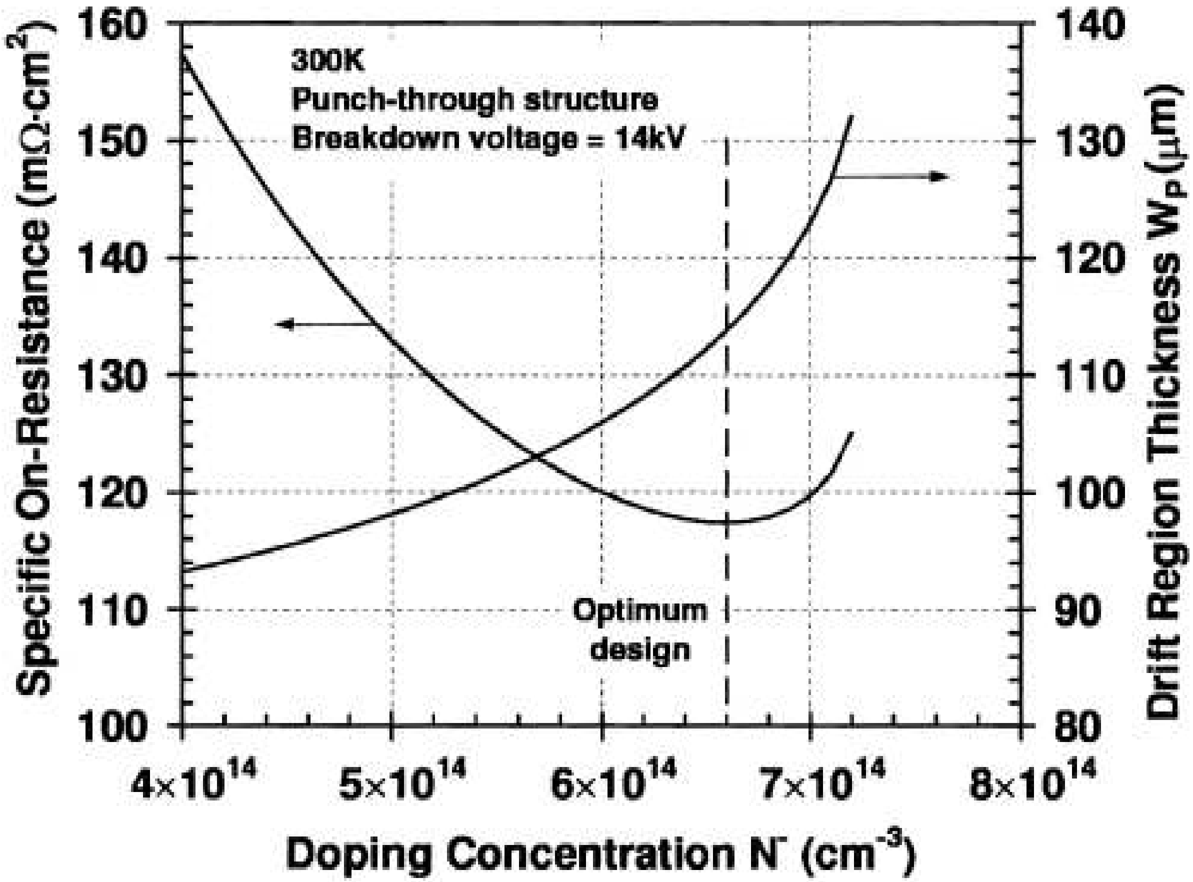

Figure 6. Optimization of the drift region doping concentration and thickness for a 14 kV punch-through structure in 4H-SiC at 300 °K.

For a given breakdown voltage, the drift region thickness and doping concentration of punch-through structure can be optimized to give the lowest specific on-resistance by using Eqs. (7), (12) and (17). Figure 6 illustrates such an optimization scheme performed for a breakdown voltage of 14 kV at 300 °K. The optimum drift region thickness and doping concentration are 114 *μm* and $6.6\times10^{14} cm^{-3}$, respectively, which gives the lowest specific on-resistance of 117 mΩcm². The optimum drift region thickness and doping concentration for 4H-SiC punch-through structure at different breakdown voltages are presented in Figure 7. And the optimum specific on-resistance is compared with the theoretical specific on-resistance of non punch-through structure in Figure 8, where the optimized punch-through structure not only has a thinner drift region, but also has a slightly lower specific on-resistance than non punch-through structure. Hence, most power devices utilize punch-through structure.

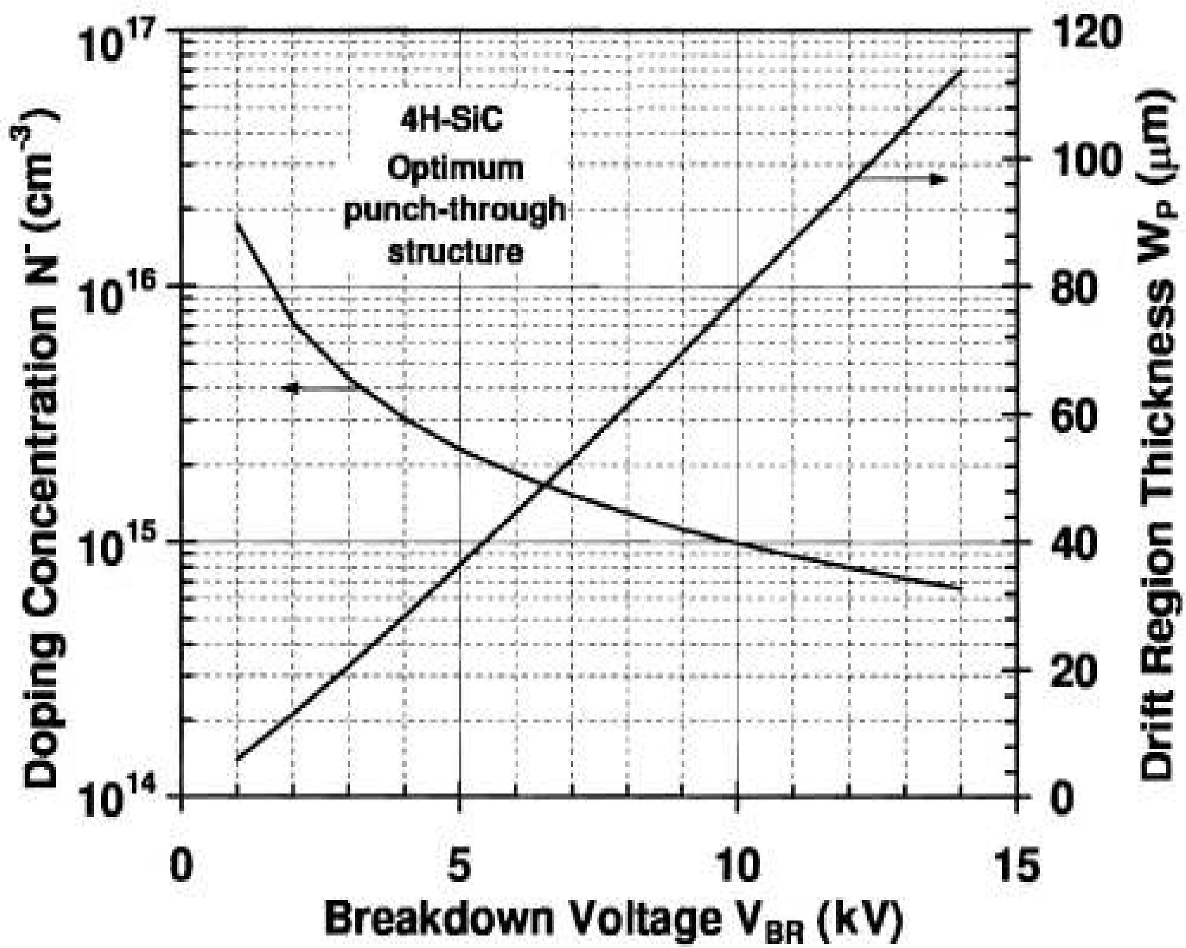

Figure 7. Optimized doping concentration and thickness for the drift region of 4H-SiC punch-through structure.

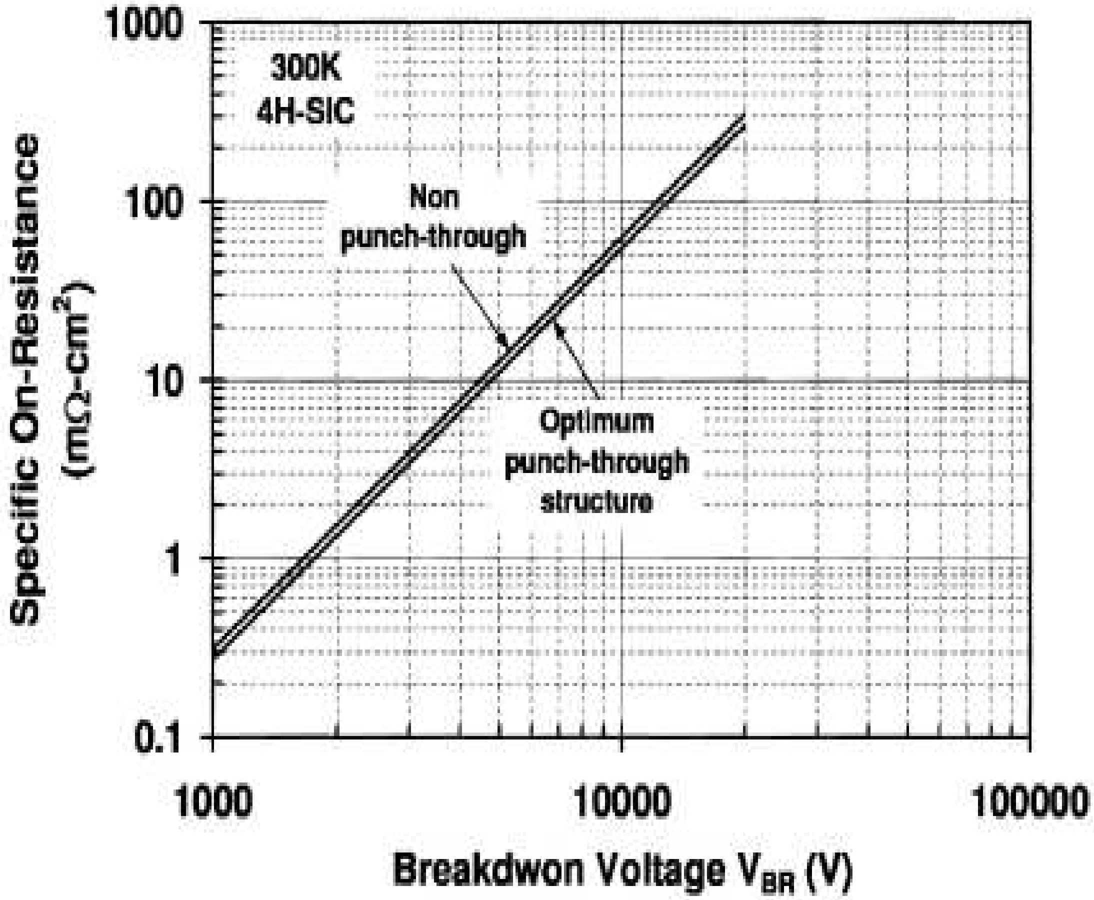

Figure 8. Comparison of the optimized specific on-resistance of 4H-SiC punch-through structure with that of non punch-through structure.

3. Comparison with Experimental Data and Discussions

The Atlas device simulator [11] is used to perform two-dimensional numerical simulations for all devices investigated in this report. Figure 9 shows the schematic cross sectional view of the 4H-SiC NPN BJT cell structure, which is studied in this research. This structure consists of three epilayers. The top N^+ layer is the emitter. The middle p-type epilayer is the base. The N^- layer (drift layer) between the N^+ collector and the P base is used to support the high breakdown voltage. The emitter mesa is etched into the P base layer by 0.2 *μm*. A thin, highly doped P^+ region can be formed by ion implantation under the base contact to reduce contact resistance. This structure is designed to be able to block near 2000 V under the optimum reach-through condition when the emitter is open. A 12 *μm*, $7\times10^{15}cm^{-3}$ doped n-type epilayer is chosen for the drift layer. To prevent the punch-through of the base, the initial base doping concentration is $3.7\times10^{17}cm^{-3}$ and the initial base width is 0.8 *μm*. The emitter has a doping concentration of $2\times10^{19}cm^{-3}$ and a thickness of 1.5 *μm*.

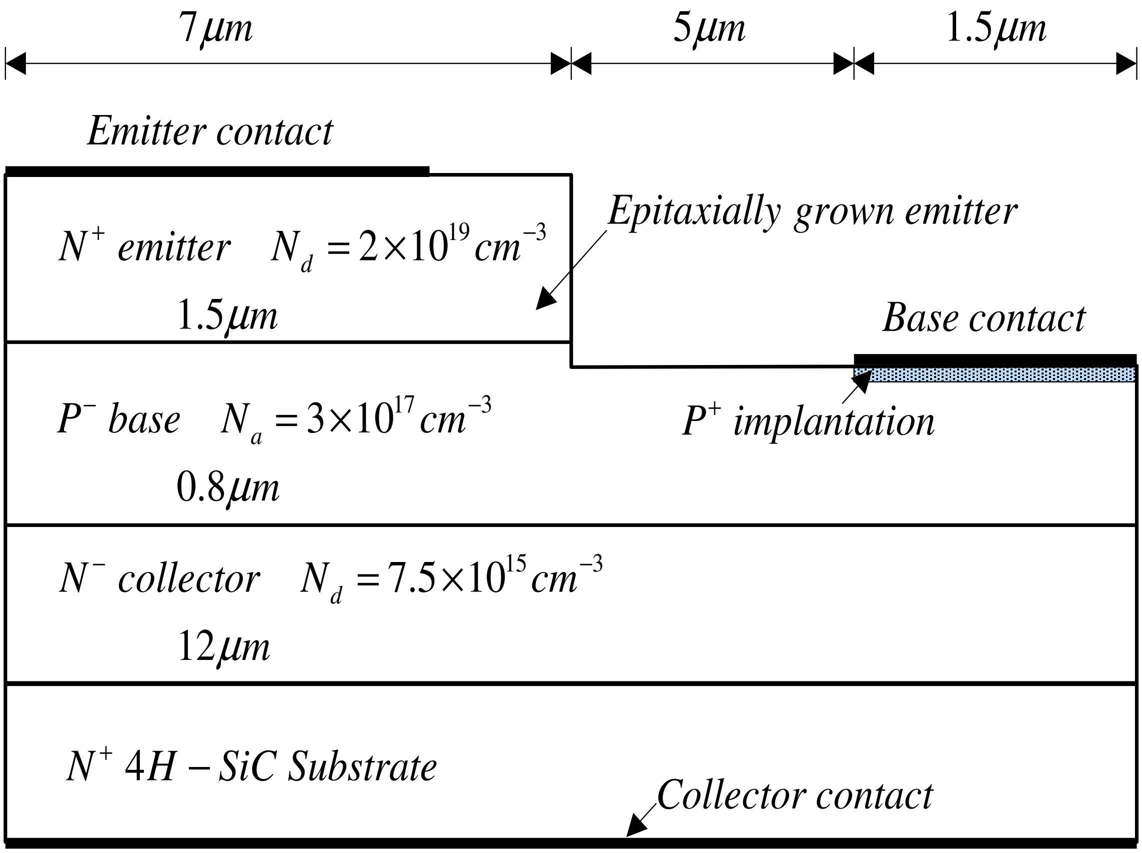

Figure 9. Schematic cross-section view of the 4H-SiC NPN BJT cell structure.

The simulated blocking characteristics of the 4H-SiC NPN BJT are shown in Figure 10. The device is able to block 1941 V and 2094 V at 300 °K and 523 °K, respectively, when the emitter is open. When the base is open, the device can block 1631 V and 2033 V at 300 °K and 523 °K, respectively. The blocking voltage is smaller when the base is due to the current-amplifying properties of the common emitter connection.

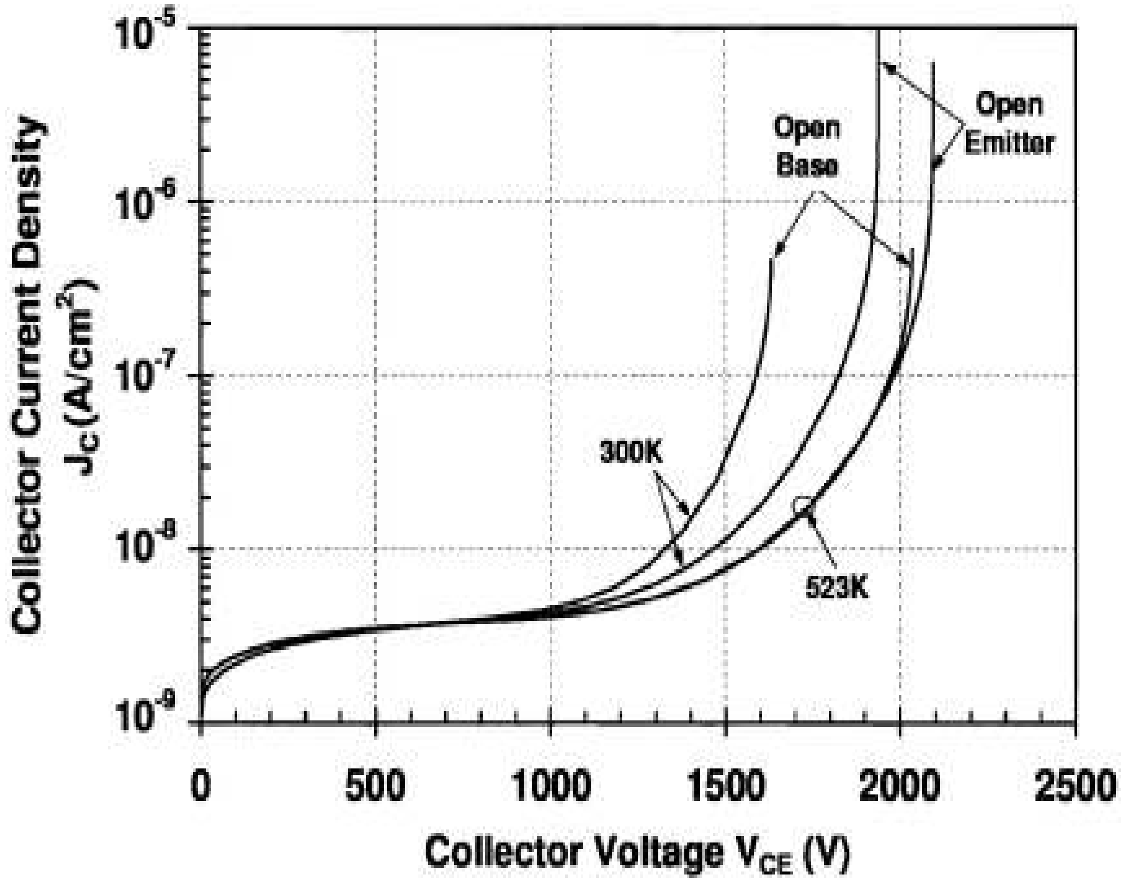

Figure 10. Simulated blocking characteristics of the 4H-SiC NPN BJT at 300 °K and 523 °K.

The structure of the experimental device is the same as the one shown in Figure 9 except that the emitter layer thickness is 0.7 *μm*. The device active area is 0.012 cm^2. The experimental data in this section is taken from [34]. The simulation parameters used in ATLAS program are given in Table 1. The measured and simulated I-V characteristics of the device at room temperature are shown in Figure 11. The collector current (I_C) is measured up to 4.41 A (current density of J_C = 368 A/cm^2) at a base current (I_B) of 140 mA, corresponding to a common emitter current gain of 31 at collector emitter voltage of V_{CE} = 8 V. The maximum current gain is 32 at J_C =319 A/cm^2. The specific on-resistance is 17 mΩcm^2 measured at V_{CE} =5 V and I_B = 140 mA. The open-base blocking voltage is near 1600V at room temperature, where the leakage current is only 1.2 mA. The leakage current in Figure 11 has been amplified by a factor of 1000 in order to show the details. This result represents state of the art for 4H-SiC NPN BJTs with both high blocking capability and high current gain at high current density.

The theoretical specific on-resistance of the experimental BJT is about 1.5 mΩcm^2 (assuming the maximum electron mobility is 947 cm^2/Vs), which is about 11 times lower than the measured specific on-resistance. The high measured specific on-resistance may not be due to the low electron mobility because the device has a high current gain. The fitting to the measured *I-V* characteristics cannot be achieved by using low electron mobility even when the maximum carrier lifetimes are as high as 5 µs. At present, it is actually not well understood why the measured specific on-resistance is so high. Thus, a resistor of 1.24 Ω is connected to the collector in order to fit the specific on-resistance of the device.

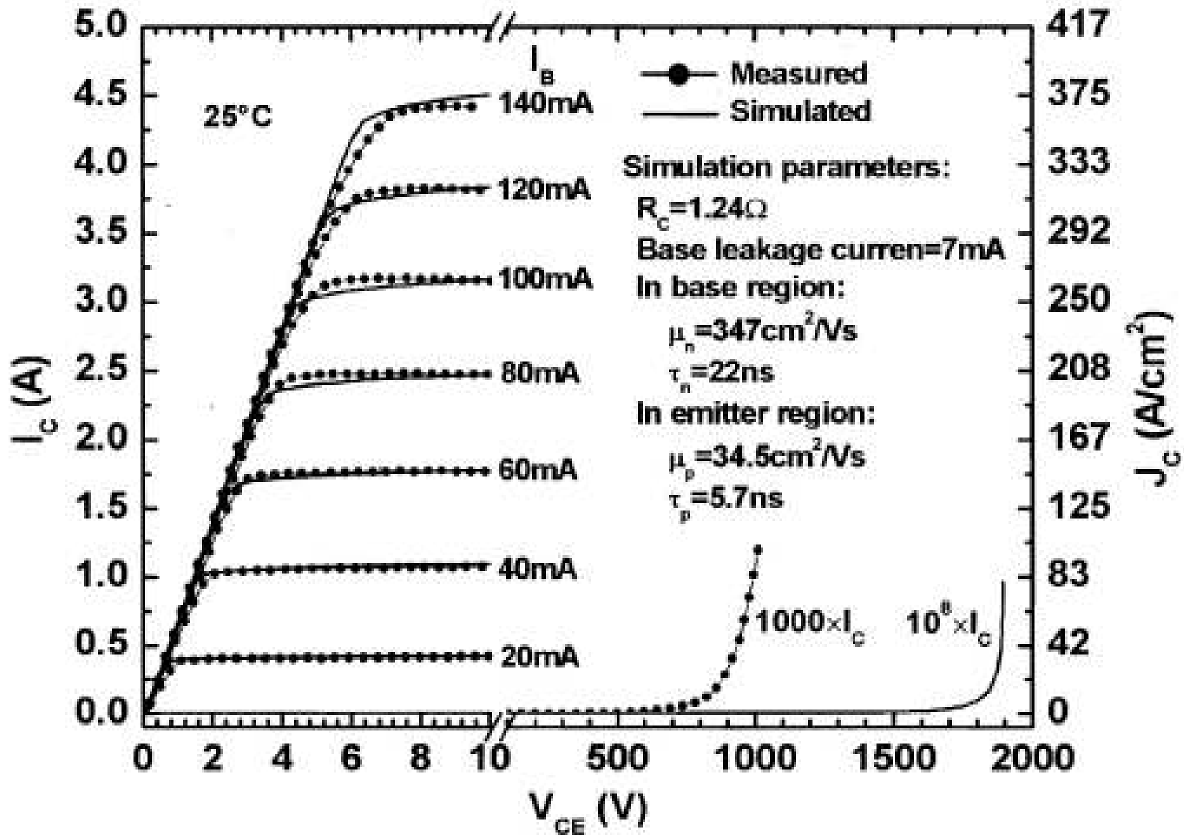

Figure 11. Measured and simulated output characteristics (I_C vs. V_{CE}) of the fabricated 4H-SiC NPN BJT at room temperature; the measured data is taken from [34].

4. Conclusion

The specific on-resistance is compared with the theoretical specific on-resistance of non punch-through structure. It is shown that the optimized punch-through structure not only has a thinner drift region, but also has a slightly lower specific on-resistance than non punch-through structure. The model is applied and compared to a measured 4H-SiC bipolar transistors with high blocking voltage and results are discussed. The experimental 4H-SiC BJT is able to block 1631 V and 2033 V at 300 °K and 523 °K when the base is open, respectively. The simulated blocking voltage when base is open is slightly lower, 1600 V at 300 °K, than the experimental value due to the current-amplifying properties of the common-emitter BJT. In 4H-SiC, there is a significant anisotropy in the electron mobility and the impact ionization coefficients. (The anisotropy, however, has not been implemented in the commercial software used in this study). In order to predict accurately the forward and blocking performance of a 4H-SiC power device, the anisotropy must be considered. There need to have more accurate physical parameters derived from measured data for 4H-SiC, such as the temperature coefficient in the impact ionization coefficients. This parameter is essential for evaluating the device performance at high temperature.

References

[1] Miyake, H., Okuda, T., Niwa, H., Kimoto, T., and Jun Suda, J., 2012. 21-kV SiC BJTs With Space-Modulated Junction Termination Extension", IEEE Electron Device Letters, vol. 33, no. 11, pp. 1598-1600.

[2] Ryu, S.H., Capell, C., Jonas, C., Cheng, L., O'Loughlin, M., Burk, A., Agarwal, A., and Palmour, J., Hefner, A., 2012. Ultra High Voltage (>12 kV), High Performance 4H-SiC IGBTs, Proceedings of the 2012 24th International Symposium on Power Semiconductor Devices and ICs, 3-7 June 2012 - Bruges, Belgium.

[3] Zetterling, C. M, 2002. Process technology for silicon carbide devices, in EMIS processing series, IEE.

[4] Chow, T. P., 2000. SiC and GaN High-Voltage Power Switching Devices, Materials Science Forum, vol.338, p. 1155.

[5] Choyke, W. J. and Pensl, G. 1997. Physical Properties of SiC, in MRS Bulletin, vol. 22, p. 25.

[6] Bhalla, A. and Chow, T.P., 1994. Bipolar Power Device Performance: dependence on materials, lifetime, Proc. of the 6th Internat. Symposium on Power Semiconductor Devices & IC's, Davos, Switzerland, May 31 - June 2, 1994, pp. 287-291.

[7] Lee, H.-S., Domeij, M., Zetterling, C.-M., OÌˆstling, M., Allerstam, F., SveinbjoÌˆrnsson, E. OÌˆ, 2008. Surface passivation oxide effects on the current gain of 4H-SiC bipolar junction transistors, Applied Physics Letters, vol. 92, no.8, pp.082113, 2008, ISSN: 00036951.

[8] Zolper, J. E., 2005. Emerging silicon carbide power electronics components, IEEE Applied Power Electronics Conference and Exposition (APEC), pp.11-17.

[9] Xiao-Yan, T., Qing-Wen, S., Yu-Ming, Z., Yi-Men, Z., Ren-Xu, J., Hong-Liang, L., and Yue-Hu, W., 2012. Investigation of a 4H SiC metal insulation semiconductor structure with an Al2O3/SiO2 stacked dielectric, Chin. Phys. B., vol. 21, no. 8, 087701.

[10] Qian, Z., Yu-Ming, Z., Lei, Y., Yi-Men, Z., Xiao-Yan, T., and Qing-Wen, S., 2012. Fabrication and characterization of 4H SiC bipolar junction transistor with double base epilayer, Chin. Phys. B., vol. 21, no. 8, 088502.

[11] Silvaco International Software, 2005. Atlas User's Manual, Santa Clara, CA, USA. [12] Yong-Hui, D., Gang, X., Tao, W., and Kuang, S., 2013. A novel 4H-SiC lateral bipolar junction transistor structure with high voltage and high current gain, Chin. Phys. B vol. 22, no. 9,097201.

[13] Pâques, G., Scharnholz, S., Dheilly, N., Planson, D., and De Doncker, R., 2011. High-Voltage 4H-SiC Thyristors With a Graded Etched Junction Termination Extension, IEEE EDS, vol. 32, no.10.

[14] Bellotti, E., Nilsson, H.E., and Brennan, K.F. 2000. Monte Carlo calculation of hole initialed impact ionization in 4H phase SiC, J. Appl. Phys., vol.87, no.8, pp. 864-3871.

[15] Niwa, H., Feng G., Suda, J., and Kimoto, T., 2012. Breakdown characteristics of 12–20 kV-class 4H-SiC PiN diodes with improved junction termination structures, Proceedings of the 2012 24th International Symposium on Power Semiconductor Devices and ICs, 3-7 June 2012 - Bruges, Belgium, pp.381-384.

[16] Imhoff, E.A., Kub, F. J., Hobart, K. D., \ Ancona, M.G., VanMil, B.L., Gaskill, D. K., Keong K.L., Myers-Ward R. L., and Eddy, Jr. C. R., 2011. High-Performance Smoothly Tapered Junction Termination Extensions for High-Voltage 4H-SiC Devices, IEEE EDS, vol. 58, no.10.

[17] Feng, G., Suda, J., and Kimoto, T., 2012. Space-Modulated Junction Termination Extension for Ultrahigh-Voltage p-i-n Diodes in 4H-SiC, IEEE EDS, vol. 59, no.2.

[18] Prasad, R., 2013. Application of Low Specific on Resistance and High Thermal Stability 6H –SIC DIMOSFET using with Uniform Distribution in the Drift Region," International Journal of Scientific and Research Publications, vol. 3, Issue 6, June 2013 1 ISSN 2250-3153.

[19] Kimura, R., Uchida, K, Hiyoshi, T., Sakai, M., Wada, K., and Mikamura, Y., 2013. SiC High Blocking Voltage Transistor, SEI Technical Review, no. 77.

[20] Qing-Wen, S., Yu-Ming, Z., Ji-Sheng, H, Tanner, P., Dimitrijev, S., Yi-Men, Z., Xiao-Yan, T., and Hui, G., 2013. Fabrication and characterization of 4H SiC power UMOSFETs, Chin. Phys. B., vol. 22, no. 2, 027302.

[21] Hatakeyama, Y., Nomoto, K., Kaneda, N., Kawano, T., Mishima, T., and Nakamura, T., 2011. Over 3.0 GW/cm2 Figure-of-Merit GaN p-n Junction Diodes on Free-Standing GaN Substrates, IEEE ED Letter, vol. 32, no.12.

[22] Hatakeyama, Y., Nomoto, K., Terano, A., Kaneda, N., Tsuchiya, AT., Mishima, TY., and Nakamu, T., 2013. High-Breakdown-Voltage and Low-Specific-on-Resistance GaN p–n Junction Diodes on Free-Standing GaN Substrates Fabricated Through Low-Damage Field-Plate Process," Japanese Journal of Applied Physics, 52, 028007.

[23] Mochizuki, K., Mishima, T., Terano, A., Kaneda, N., Ishigaki, T., and Tsuchiya, T., 2011, Numerical Analysis of Forward-Current/Voltage Characteristics of Vertical GaN Schottky Barrier Diodes and p-n Diodes on Free-Standing GaN Substrates, IEEE EDS, vol. 58, no.7.

[24] Nomoto, K., Hatakeyama, Y., Katayose, H., Kaneda, N., Mishima, T., and Nakamura, T., 2011. Over 1.0 kV GaN p–n junction diodes on free-standing GaN substrates, Phys. Status Solidi A 208, no. 7, 1535–1537.

[25] Ryu, S. H., Agarwal, A. K., Singh R., and Palmour, J. W. 2001. 1800V NPN bipolar junction transistors in 4H-SiC, IEEE Electron Device Letters, vol. 22, p. 124.

[26] Zhang, J., Zhao, J.H., Alexandrov, P., and Burke, T., 2004. Demonstration of first 9.2kV 4H-SiC bipolar junction transistor, Electronics Letters, vol. 40, p. 1381.

[27] Zhang, J., Alexandrov, P., T. Burke, and Zhao, J. H., 2006. 4H-SiC power bipolar junction transistor with a very low specific on-resistance of 2.9 mΩcm^2, IEEE Electron Device Letters, vol. 27, p. 368.

[28] Chynoweth, G., 1958. Ionization rates for electrons and holes in Silicon, Physics Review, vol. 109, no.5, pp. 1537-40.

[29] Raghunatha, R., and Baliga, B.J., 1999. Temperature dependence of hole impact ionization coefficients in 4H and 6H-SiC, Solid-States Electronics, vol.43, pp.199-211.

[30] Yokuto, Y., and Crowell, C.R., 1975. Threshold energy effects on avalanche breakdown voltage in semiconductor junctions, Solid-States Electronics, vol. 18, pp.161-168.

[31] Konstantinov, A.O., Wahab, Q., Nordell, N., and Lindefelt, U., 1997. Ionization rates and critical fields in 4H silicon carbide, Appl. Phys. Lett., 71(1), 90-92.

[32] Baliga, B.J., 1987. Modern Power Devices, New York: Wiley, 1987.

[33] Niu, X., 2010. Design and Simulation of 4H Silicon Carbide Power Bipolar Junction Transistors, MSEE thesis, University of Colorado, Denver.

[34] Luo, Y., Zhang, J.H., Alexandrov, P., Fursin, L. , Zhao, J.H., and Burke, T. 2003. High voltage (>lkV) and high current gain (32) 4H-SiC power BJTs using Al-free ohmic contact to the base, IEEE Electron Devices Letters, vol.24, no.11, pp.695-697.